Journal of Physics: Complexity

Check for updates

PAPER

OPEN ACCESS

RECEIVED
16 June 2026

REVISED
15 September 2026

ACCEPTED FOR PUBLICATION
6 October 2026

PUBLISHED
16 October 2026

Original content from this work may be used under the terms of the Creative Commons Attribution 4.0 licence.

Any further distribution of this work must maintain attribution to the author(s) and the title of the work, journal citation and DOI.

Noise seeded oscillators: on the role of demographic fluctuations in a multi-populations model

Francesca Di Patti[1,3,4,*], **Duccio Fanelli**[2,3,4] and **Perla Rosi**[1]

[1] Dipartimento di Matematica e Informatica 'Ulisse Dini', Universitá degli Studi di Firenze, viale Morgagni 67/a, 50134 Firenze, Italy
[2] Dipartimento di Fisica e Astronomia, Universitá degli Studi di Firenze, via G. Sansone 1, 50019 Sesto Fiorentino, Italy
[3] INFN, Sezione di Firenze, via G. Sansone 1, 50019 Sesto Fiorentino, Italy
[4] CSDC—Centro Interdipartimentale per lo Studio delle Dinamiche Complesse, via G. Sansone 1, 50019 Sesto Fiorentino, Italy
[*] Author to whom any correspondence should be addressed.

E-mail: francesca.dipatti@unifi.it

Keywords: stochastic quasi-cycles, Langevin equations, computational neuroscience

Abstract

Stochastic oscillations can emerge in two-population models as a consequence of endogenous finite-size fluctuations. Here, we investigate how the introduction of a third fluctuating species, representing an additional interacting population, affects the stochastic dynamics of a prototypical model of neuronal interactions. Our results show that the presence of this additional species can substantially modify the collective behavior of the neuronal populations. When the characteristic sizes of the neuronal populations and the third species are of the same order, the latter modifies the characteristic frequency of the noise-induced quasi-cycles and can ultimately suppress their emergence. Conversely, when the neuronal populations are more abundant than the characteristic size of the third species, the latter enhances the effective noise acting on the neuronal populations, thereby amplifying their stochastic fluctuations. These results demonstrate that an additional population can qualitatively alter noise-induced collective dynamics, either modulating or suppressing coherent stochastic oscillations or enhancing the strength of demographic fluctuations. More generally, our findings point to the importance of accounting for intermediate stochastic populations when modeling interacting noisy oscillators and provide a framework for investigating how additional sources of fluctuations affect collective dynamics and synchronization beyond the classical Kuramoto setting.

1. Introduction

The study of synchronization phenomena has become a central topic in the analysis of complex systems, as coordinated behavior emerges across a broad range of natural and artificial systems, including neural populations, biological rhythms, power grids, and social interactions [19, 22]. Among the theoretical frameworks developed to understand collective synchronization, the Kuramoto model has played a pivotal role [27]. Introduced as a minimal yet analytically tractable description of coupled oscillators, the Kuramoto model captures how a population of heterogeneous units can spontaneously move from incoherent dynamics to collective synchronization through interactions. Its simplicity and versatility have made it a paradigmatic model for investigating synchronization transitions, collective behaviors, and self-organized phenomena in complex systems [1, 11, 21]. The Kuramoto model, and its main alternatives, focus on phase synchronization. This latter often assumes amplitude to be constant or irrelevant (as e.g. in the classic Kuramoto model). But in real oscillators, amplitude dynamics matter immensely. True oscillators have amplitude stability, which phase synchronization models often gloss over. As a relevant example, in biological contexts, and specifically in neuroscience, collective dynamics arise from interactions between populations of homologous entities whose activity is governed not only by phase relationships but it is primarily instigated by the nonlinear excitation and inhibition loops [9]. In this context, neural mass models provide a more suitable mesoscopic description of individual oscillators,

© 2026 The Author(s). Published by IOP Publishing Ltd

and their emerging orchestrated dynamics. Among different dynamical schemes in computational neuroscience, the Wilson–Cowan model stands as a cornerstone framework to illustrate the temporal evolution of interacting excitatory and inhibitory neuronal populations [23, 24]. By incorporating nonlinear population responses and feedback mechanisms, the Wilson–Cowan model offers a rich description of collective neural activity and bridges microscopic interactions with macroscopic emergent dynamics. As such, it has become the reference standard in the theoretical description of neural population dynamics, providing insight into a broad spectrum of collective neural phenomena, ranging from visual hallucinations and binocular rivalry to pathological states such as epilepsy [25]. Owing to its versatility and analytical tractability, it is now regarded as one of the most influential mean-field models in theoretical neuroscience. Despite its success, the original formulation of the model is entirely deterministic and therefore neglects the effects of stochasticity. Accounting for fluctuations is however mandatory from a wide biological perspective: noise can in fact play a fundamental dynamical role by triggering collective response rather than representing a mere source of undesired perturbation [17]. In particular, intrinsic fluctuations may actively induce self-organized behaviors even in parameter regions where the deterministic dynamics predicts a stable fixed point [2, 6, 14, 18]. Motivated by these observations, stochastic reformulations of the Wilson–Cowan framework have been proposed [5]. Among these, recent studies have shown that endogenous fluctuations originating from the finite size of the system can seed synchronized quasi-cycles in excitatory populations distributed across network nodes [8, 28]. These findings emphasize the constructive role that demographic noise may play in shaping collective neural dynamics. This contribution is indeed positioned in this setting and aims at further elucidating the emergence of complex, seemingly regular, oscillations as sustained by the intrinsic finite size noise. Beyond the case here explored, the coupled dynamics of the noise triggered oscillators could be considered as a generalized framework of possible exploration, beyond phase oscillator models inspired to the seminal work of Kuramoto.

A limitation of the standard stochastic formulation is that it generally relies on the assumption of moderate or low copy numbers for the interacting species. While this assumption is natural in many biochemical contexts, its applicability to neuronal populations may be less immediate and can therefore raise conceptual and modeling concerns. Nevertheless, neurons or, more generally, interacting biological units, often communicate through intermediary chemical species whose concentrations may indeed be sufficiently small for stochastic effects to become relevant, even when the neuronal populations themselves are large [12, 15]. In such situations, stochasticity is essential only for a subset of the dynamical variables, whereas the remaining degrees of freedom may still be accurately described within a deterministic framework [4, 26].

The aim of the present work is therefore to investigate hybrid dynamical scenarios in which stochastic variables with different characteristic sizes coexist and interact. In particular, we seek to determine whether fluctuations acting only on a subset of the system variables are sufficient to sustain or suppress the emergence of quasi-cycles, the coherent oscillation stimulated by the endogenous noise component.

The paper is organized as follows. The next section introduces the model under investigation and discusses the differences between its deterministic and stochastic descriptions. Section 3 focuses on the role of the third species and shows how its presence can prevent the emergence of stochastic oscillations. In section 4, we perform an adiabatic elimination of the third species and investigate the resulting effective description. Finally, in the last section, we summarize the main results and conclusions of the work.

2. The three-species stochastic model

We consider an extension of the single-node model originally introduced in [28] in the context of neuroscience. The model describes the dynamics of two interacting neuronal populations composed of individuals of type X and Y, where X denotes excitatory neurons and Y inhibitory ones. In the present work, we extend the original framework by introducing additional interactions mediated by a third species, denoted by Z. The introduction of this additional species is motivated by the fact that, as anticipated in the Introduction, neuronal interactions are not mediated exclusively by direct electrical coupling but can also occur through chemical signaling. In particular, a fundamental mechanism of communication between neurons is provided by chemical synapses, where the electrical activity of a presynaptic neuron is converted into a chemical signal through the release of neurotransmitter molecules into the synaptic cleft. The released neurotransmitters subsequently diffuse across the synaptic cleft and bind to specific receptors on the postsynaptic neuron, thereby modifying its membrane conductance and, consequently, its electrical activity [20]. From a modeling perspective, this provides a natural motivation for explicitly including an additional chemical species in the dynamical system. Such a variable can represent, at an

effective level, the concentration or abundance of a neurotransmitter or other signaling molecule sensed by the neural populations. In this way, the model distinguishes between the dynamics of the neuronal populations themselves and that of the chemical mediator through which they interact. This extension naturally introduces two distinct characteristic size parameters into the system: a volume V associated with the neuronal populations X and Y, and a different volume V_1 associated with the chemical species Z. Although V and V_1 formally enter the model as parameters characterizing the size of the system, they should not necessarily be interpreted literally as the physical number of individuals. Rather, they can be regarded more generally as effective measures of the characteristic size of the corresponding populations. Depending on the physical interpretation of the model, these quantities may be related, for example, to the volume or area occupied by the corresponding species, or to the characteristic number of molecules present in the relevant spatial domain [16]. The introduction of two distinct characteristic sizes is particularly useful because it allows to disentangle the effects of fluctuations associated with the neuronal populations from those associated with the chemical mediator. In particular, by varying V and V_1 independently, one can investigate regimes in which demographic fluctuations predominantly affect the neuronal populations, the chemical species, or both. This distinction is physically reasonable because neurons and signaling molecules can occur at vastly different characteristic abundances and therefore naturally give rise to different scales of fluctuations.

To introduce the stochastic model, we formulate the system in terms of chemical reactions, following the standard formalism commonly used in stochastic modeling. In particular, the stochastic dynamics of the X and Y populations is governed by the same set of reactions as in [28]:

$$\begin{aligned} X &\xrightarrow{1} \varnothing \\ Y &\xrightarrow{1} \varnothing \\ \varnothing &\xrightarrow{f(s_x)} X \\ \varnothing &\xrightarrow{f(s_y)} Y \end{aligned} \tag{1}$$

where $f(s)$ is a sigmoid function which can be cast in the form:

$$f(s) = \frac{1}{1 + be^{-s}} \tag{2}$$

whose steepness is controlled by the parameter b. The arguments of the sigmoid are given by

$$\begin{aligned} s_x &= -r\left(\frac{n_y}{V} - \frac{1}{2}\right) \\ s_y &= r\left(\frac{n_x}{V} - \frac{1}{2}\right) \end{aligned}$$

with r a positive free parameter and n_x, n_y denoting the instantaneous numbers of X and Y individuals, respectively. The symbol $\varnothing$ appearing in equation (1) denotes an infinite reservoir. Accordingly, the first two chemical reactions describe the loss of excitatory and inhibitory neurons from the respective populations, while the last two reactions represent the feedback interactions between the two neuronal populations. In particular, a large inhibitory population suppresses the excitatory population, whereas a large excitatory population promotes the growth of the inhibitory population. The latter interaction is mediated by a sigmoid function, which naturally accounts for the threshold-like response of neuronal populations.

To account for the possible modulation of neuronal activity by extracellular chemical signals, we introduce an additional species Z, which, as discussed above, represents a diffusible inhibitory neuromodulatory substance. To establish a connection with a biologically relevant example, we can consider adenosine, a molecule that can exert a predominantly inhibitory and homeostatic effect on neuronal activity through activation of specific receptors. In particular, extracellular adenosine provides tonic inhibition of neuronal networks and contributes to the regulation of neuronal excitability [3, 7]. Its extracellular concentration is determined by a balance between production/release and removal through cellular uptake and metabolic degradation [13]. Accordingly, the reactions

$$\begin{aligned} Z &\xrightarrow{\delta_z} \varnothing, \\ \varnothing &\xrightarrow{\alpha_z} Z \end{aligned} \tag{3}$$

represent, respectively, the effective production of the neuromodulatory species and its clearance from the local extracellular environment. The latter may include enzymatic degradation, cellular uptake, or transport out of the considered volume. The inhibitory interactions between Z and the two neuronal populations are instead represented by

$$\begin{aligned} X+Z &\xrightarrow{\gamma} Z \\ Y+Z &\xrightarrow{\gamma} Z. \end{aligned} \tag{4}$$

This catalytic representation captures the action of an extracellular neuromodulator that modifies neuronal excitability through receptor-mediated mechanisms without being stoichiometrically consumed.

The stochastic dynamics of the state vector $\mathbf{n}(t) = (n_x(t), n_y(t), n_z(t))$ is ruled by the master equation, the differential equation for the probability $P(\mathbf{n}, t)$ of observing the system in the state $\mathbf{n}$ at time t. Its generic form reads

$$\frac{\mathrm{d}P}{\mathrm{d}t}(\mathbf{n}, t) = \sum_{\mathbf{n}\neq\mathbf{n}'} T(\mathbf{n}|\mathbf{n}')P(\mathbf{n}', t) - T(\mathbf{n}'|\mathbf{n})P(\mathbf{n}, t) \tag{5}$$

where $T(\mathbf{n}|\mathbf{n}')$ denotes the probability rate that the system undergoes the transition $\mathbf{n}' \to \mathbf{n}$. According to the chemical reactions (1), (3) and (4), the explicit form of the transition rates are

$$\begin{aligned} T\left(n_x-1, n_y, n_z|\mathbf{n}\right) &= \frac{n_x}{V} + \gamma\frac{n_x}{V}\frac{n_z}{V_1} \\ T\left(n_x, n_y-1, n_z|\mathbf{n}\right) &= \frac{n_y}{V} + \gamma\frac{n_y}{V}\frac{n_z}{V_1} \\ T\left(n_x, n_y, n_z-1|\mathbf{n}\right) &= \frac{n_z}{V_1}\delta_z \\ T\left(n_x, n_y, n_z+1|\mathbf{n}\right) &= \alpha_z \end{aligned} \quad . \tag{6}$$

Multiplying both sides of equation (5) by, respectively n_x, n_y and n_z, and summing over $\mathbf{n}$ one can derive the equations governing the average quantities $\langle n_l\rangle = \sum_{\mathbf{n}} n_l P(\mathbf{n}, t)$ for $l = x, y, z$:

$$\begin{cases} \frac{\mathrm{d}}{\mathrm{d}t}\langle n_x\rangle = \langle f(s_x)\rangle - \left\langle \frac{n_x}{V}\right\rangle - \gamma\left\langle \frac{n_x}{V}\frac{n_z}{V_1}\right\rangle \\ \frac{\mathrm{d}}{\mathrm{d}t}\langle n_y\rangle = \langle f(s_y)\rangle - \left\langle \frac{n_y}{V}\right\rangle - \gamma\left\langle \frac{n_y}{V}\frac{n_z}{V_1}\right\rangle \\ \frac{\mathrm{d}}{\mathrm{d}t}\langle n_z\rangle = \alpha_z - \delta_z\left\langle \frac{n_z}{V_1}\right\rangle. \end{cases} \tag{7}$$

As is customary in stochastic modeling, the previous equation can be associated with a corresponding mean-field equation describing the deterministic behavior of the system. To this end, we introduce the deterministic concentrations x, y and z, defined as

$$x = \lim_{V\to+\infty}\left\langle \frac{n_x}{V}\right\rangle, \quad y = \lim_{V\to+\infty}\left\langle \frac{n_y}{V}\right\rangle, \quad z = \lim_{V_1\to+\infty}\left\langle \frac{n_z}{V_1}\right\rangle. \tag{8}$$

The deterministic equations are then obtained by substituting these quantities into equation (5) and taking the limits $V \to \infty$ and $V_1 \to \infty$. In this limit, the fluctuations become negligible and the stochastic concentrations n_x/V, n_y/V, and n_z/V_1 can be replaced by their corresponding deterministic values x, y and z, respectively. Moreover, correlations between the stochastic variables become negligible in the deterministic limit. In particular, the joint moments can be approximated by products of the corresponding mean concentrations, so that $\left\langle \frac{n_x}{V}\frac{n_z}{V_1}\right\rangle = xz$ (and the same for $\left\langle \frac{n_y}{V}\frac{n_z}{V_1}\right\rangle$). Similarly, nonlinear functions of the stochastic variables can be evaluated at their deterministic mean values, i.e. $\langle f(\cdot)\rangle = f(\langle\cdot\rangle)$. These approximations correspond to the leading-order deterministic description obtained within the van Kampen system-size expansion, in which stochastic fluctuations appear as higher-order

corrections to the macroscopic dynamics. Under these assumptions, equation (7) reduces to the following deterministic mean-field equations:

$$\begin{cases} \dfrac{\mathrm{d}x}{\mathrm{d}\tau_1} = \left[f\left(-r\left(y-\dfrac{1}{2}\right)\right) - x - \gamma xz\right]\dfrac{V_1}{V} \\ \dfrac{\mathrm{d}y}{\mathrm{d}\tau_1} = \left[f\left(r\left(x-\dfrac{1}{2}\right)\right) - y - \gamma yz\right]\dfrac{V_1}{V} \\ \dfrac{\mathrm{d}z}{\mathrm{d}\tau_1} = \alpha_z - \delta_z z. \end{cases} \tag{9}$$

The appearance of the ratio V_1/V in the first two equations of system (9) originates from the introduction of the rescaled time variable $\tau_1 = t/V_1$. From the system of equations (9), it follows immediately that the variable z admits a steady state given by $z^* = \dfrac{\alpha_z}{\delta_z}$ while the remaining variables display equilibrium solutions specified by conditions $x^* = y^* = \dfrac{1}{2}$, as in the original model, provided the parameter b of the sigmoidal function (2) satisfies $b = \dfrac{1-\gamma z^*}{1+\gamma z^*}$. This is the setting that we shall adopt in the following. Since the parameter b must be positive, this condition is fulfilled only if the following constraint holds:

$$1 - \gamma\frac{\alpha_z}{\delta_z} \rangle 0\,. \tag{10}$$

The stability of the aforementioned equilibrium point can be assessed by computing the eigenvalues of the Jacobian matrix associated with system (9):

$$\mathscr{J}\,(x^*, y^*, z^*) = \frac{V_1}{V}\begin{pmatrix} -1-\gamma\dfrac{\alpha_z}{\delta_z} & -\dfrac{r}{4}\left(1-\gamma^2\dfrac{\alpha_z^2}{\delta_z^2}\right) & -\dfrac{\gamma}{2} \\ \dfrac{r}{4}\left(1-\gamma^2\dfrac{\alpha_z^2}{\delta_z^2}\right) & -1-\gamma\dfrac{\alpha_z}{\delta_z} & -\dfrac{\gamma}{2} \\ 0 & 0 & -\delta_z\dfrac{V}{V_1} \end{pmatrix}. \tag{11}$$

The above Jacobian matrix admits a real negative eigenvalue $\lambda_1 = -\delta_z$, and a pair of complex conjugate eigenvalues $\lambda_{2,3} = \dfrac{V_1}{V}\left[-1-\gamma\dfrac{\alpha_z}{\delta_z} \pm \mathrm{i}\dfrac{r}{4}\left(1-\gamma^2\dfrac{\alpha_z^2}{\delta_z^2}\right)\right]$. Since the real parts of all eigenvalues are negative, the equilibrium point is asymptotically stable. Importantly, however, the presence of a non-zero imaginary part opens the possibility for stochastic oscillations around the fixed point. Although the deterministic dynamics exhibits damped oscillations, intrinsic noise can sustain these fluctuations, giving rise to so-called quasi-cycles.

To investigate this possibility, we apply the system-size expansion to the stochastic system. Following the derivation detailed in section A, we obtain a set of nonlinear Langevin equations:

$$\begin{cases} \dfrac{\mathrm{d}x}{\mathrm{d}\tau_1} = \dfrac{V_1}{V}\left(f(s_x) - x - \gamma xz\right) + \dfrac{1}{\sqrt{V_1}}\dfrac{V_1}{V}\sqrt{x+\gamma xz+f(s_x)}\;\lambda^{(1)} \\ \dfrac{\mathrm{d}y}{\mathrm{d}\tau_1} = \dfrac{V_1}{V}\left(f(s_y) - y - \gamma yz\right) + \dfrac{1}{\sqrt{V_1}}\dfrac{V_1}{V}\sqrt{y+\gamma yz+f(s_y)}\;\lambda^{(2)} \\ \dfrac{\mathrm{d}z}{\mathrm{d}\tau_1} = \alpha_z - z\delta_z + \dfrac{1}{\sqrt{V_1}}\sqrt{z\delta_z+\alpha_z}\;\lambda^{(3)}. \end{cases} \tag{12}$$

To check if the deterministic and stochastic descriptions of the system exhibit markedly different dynamical behaviors we performed numerical simulations summarized in figure 1. In the deterministic limit, the system converges to the stationary state, with the concentrations of species approaching their corresponding equilibrium values. Thus, in the absence of fluctuations, the model does not display sustained oscillations: any perturbation from the stationary state is eventually damped, and the system settles into the stable equilibrium. The situation changes substantially when intrinsic fluctuations are

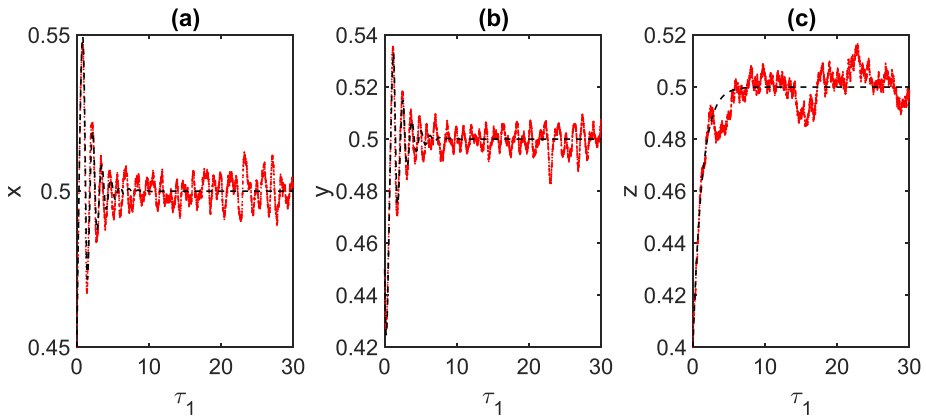


Figure 1. Comparison between the numerical integration of equation (9) (dashed black line) and equation (12) (red points). The parameters of the model are set as $r = 50$, $\gamma = 0.9$, $\alpha_z = 0.4$, $\delta_z = 0.8$, $V = 200$ and $V_1 = 100$. The differential equations are integrated numerically starting from the initial condition [0.45 0.45 0.4] using a time step $\delta_{\tau_1} = 0.025$. The stochastic differential equation (12) has been integrated through the Euler–Maruyama method [10].

taken into account. Numerical realizations of the stochastic system display persistent, quasi-regular oscillations around the deterministic stationary state. In particular, the X and Y populations exhibit sustained stochastic oscillations even though the corresponding deterministic trajectories converge to equilibrium. These oscillations therefore do not originate from an unstable or oscillatory deterministic fixed point, but are generated and maintained by the intrinsic fluctuations of the stochastic system. This behavior is characteristic of noise-induced quasi-cycles, in which demographic fluctuations continuously excite the damped oscillatory modes of the deterministic dynamics. The next sections are devoted to the analytical characterization of this phenomenon.

3. Role of species Z in preventing oscillations

We now want to investigate how the emergent dynamics is affected by the intrinsic noise component as associated to the third species. This latter acts as a sort of external (stochastic) mediator which can self-consistently modulate the inherent dynamics of the paired neuronal populations X and Y. For the above purpose we put forward the following ansatz

$$
\begin{aligned}
x &= \left(\lim_{V\to+\infty}\frac{n_x}{V}\right) + \frac{\xi_x}{\sqrt{V_1}} = \frac{1}{2} + \frac{\xi_x}{\sqrt{V_1}} \\
y &= \left(\lim_{V\to+\infty}\frac{n_y}{V}\right) + \frac{\xi_y}{\sqrt{V_1}} = \frac{1}{2} + \frac{\xi_y}{\sqrt{V_1}} \\
z &= \left(\lim_{V_1\to+\infty}\frac{n_z}{V_1}\right) + \frac{\xi_z}{\sqrt{V_1}} = \frac{\alpha_z}{\delta_z} + \frac{\xi_z}{\sqrt{V_1}}
\end{aligned}
$$

and expand the system in terms of $1/\sqrt{V_1}$. Following the detailed derivation reported in section B, we end up with a system of coupled linear Langevin equations for the vector of fluctuations $\boldsymbol{\zeta} = (\xi_x, \xi_y, \xi_z)$, namely:

$$
\frac{\mathrm{d}\zeta_i}{\mathrm{d}\tau_1} = (\mathscr{J}\zeta)_i + G_i\lambda^{(i)} \tag{13}
$$

where the matrix G reads

$$
G = \begin{pmatrix}
\frac{V_1}{V}\sqrt{1+\gamma\frac{\alpha_z}{\delta_z}} & 0 & 0 \\
0 & \frac{V_1}{V}\sqrt{1+\gamma\frac{\alpha_z}{\delta_z}} & 0 \\
0 & 0 & \sqrt{2\alpha_z}
\end{pmatrix} \tag{14}
$$

while $\mathscr{J}$ is the matrix defined by equation (11). The term $\lambda^{(i)}$ denotes the ith component of the three-dimensional vector $\boldsymbol{\lambda}$ whose elements are Gaussian white noise variables with unit variance.

Equation (13) can be solved in Fourier space. Applying the temporal Fourier transform we get

$$-\mathrm{i}\omega_{\tau_1}\tilde{\zeta}_i(\omega_{\tau_1}) = \left(\mathscr{J}\tilde{\zeta}\right)_i + G_i\tilde{\lambda}^{(i)}, \tag{15}$$

and, defining the matrix $\Phi = -\mathscr{J} - \mathrm{i}\omega_{\tau_1}\mathbb{I}_3$ where $\mathbb{I}_3$ is the 3×3 identity matrix and collecting the noise terms in the vector $\tilde{\boldsymbol{\zeta}}$, the solution of equation (15) is

$$\tilde{\boldsymbol{\zeta}}(\omega_{\tau_1}) = \Phi^{-1}G\tilde{\boldsymbol{\lambda}} \quad . \tag{16}$$

With this solution we can evaluate the power spectrum density matrix whose entries are

$$P_{ij}(\omega_{\tau_1}) = \langle\tilde{\zeta}_i(\omega_{\tau_1})\,\tilde{\zeta}_j^*(\omega_{\tau_1})\rangle = \left(\Phi^{-1}GG^t\left(\Phi^{-1}\right)^\dagger\right)_{ij} \tag{17}$$

where the indices $i,j = 1,2,3$ label the species, corresponding to X, Y and Z, respectively. The explicit form of matrix Φ is:

$$\Phi = \begin{pmatrix} \frac{V_1}{V}\left(1+\gamma\frac{\alpha_z}{\delta_z}\right) - \mathrm{i}\omega_{\tau_1} & \frac{V_1}{V}\frac{r}{4}\left(1-\gamma^2\frac{\alpha_z^2}{\delta_z^2}\right) & \gamma\frac{V_1}{2V} \\ -\frac{V_1}{V}\frac{r}{4}\left(1-\gamma^2\frac{\alpha_z^2}{\delta_z^2}\right) & \frac{V_1}{V}\left(1+\gamma\frac{\alpha_z}{\delta_z}\right) - \mathrm{i}\omega_{\tau_1} & \gamma\frac{V_1}{2V} \\ 0 & 0 & \delta_z - \mathrm{i}\omega_{\tau_1} \end{pmatrix}.$$

Following the argument introduced in [14], the position of the peak of the power spectrum can be inferred by minimizing the denominator of the power spectrum. In this specific case, the relevant quantity can be explicitly written as:

$$\det(\Phi)\det\left(\Phi^\dagger\right) = \left(\delta_z^2+\omega_{\tau_1}^2\right)\left\{\left[\omega_{\tau_1}^2 - A\right]^2 + 2\omega_{\tau_1}^2 B + C\right\} \tag{18}$$

with

$$A = \frac{r^2}{16}\frac{V_1^2}{V^2}\left(1-\gamma^2\frac{\alpha_z^2}{\delta_z^2}\right)^2$$
$$B = \frac{V_1^2}{V^2}\left(1+\gamma\frac{\alpha_z}{\delta_z}\right)^2$$
$$C = \frac{V_1^4}{V^4}\left(1+\gamma\frac{\alpha_z}{\delta_z}\right)^4\left[1+\frac{r^2}{8}\left(1-\gamma\frac{\alpha_z}{\delta_z}\right)\right].$$

Expression (18) is minimized for $\omega_{\tau_1}^2 \approx A$, that is for

$$\omega_{\tau_1} \approx \omega_{\tau_1}^* = \frac{r}{4}\frac{V_1}{V}\left(1-\gamma^2\frac{\alpha_z^2}{\delta_z^2}\right) \tag{19}$$

which is positive defined in light of the constraint imposed by equation (10).

Figure 2 shows the agreement between the power spectrum obtained through the linear noise approximation (equation (17)) and the stochastic simulations. This agreement confirms that the linear noise approximation correctly captures the main statistical features of the stochastic dynamics. It is also evident that the estimate provided by equation (19) accurately predicts the position of the spectral peak (see the dashed vertical lines as reported in panels (a) and (b) of figure 2). The presence of a well-defined peak confirms that the fluctuations in species X and Y are not purely random, but are characterized by a preferred frequency associated with the damped oscillatory modes of the deterministic system. Notably, and as expected, the power spectrum for species Z does not exhibit any peak, indicating that the noisy signal observed in figure 1(c) consists of simple fluctuations, superposed to the deterministic mean-field trajectory, rather than quasi-cycles. This is in agreement with the fact that the eigenvalue associated with the third species is real and negative, thus it does not provide a characteristic frequency to be sustained by intrinsic noise. Consequently, this mode is purely relaxational and does not introduce a characteristic frequency that can be sustained or amplified by intrinsic noise. Therefore, unlike the

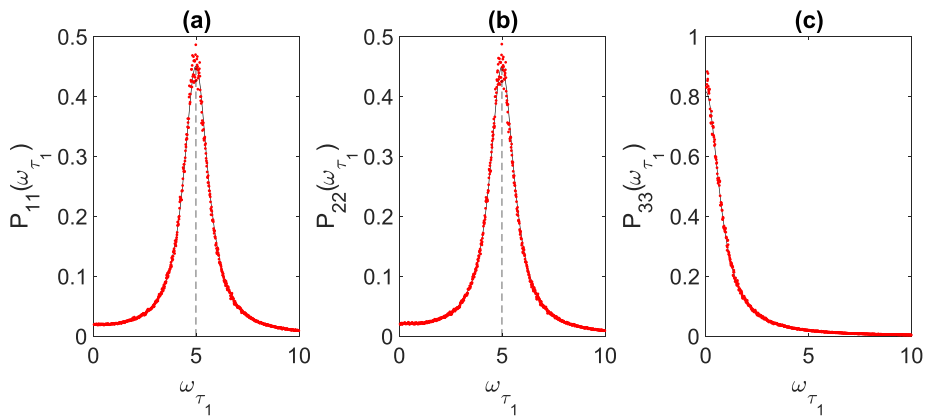


Figure 2. Comparison between the theoretical power spectrum (solid black line) obtained through the linear noise approximation (equation (17)), and numerical simulations (red points), computed by averaging over 500 independent realizations of the Langevin equation (12). Panel (a) refers to species X, (b) is relative to species Y while panel (c) shows the power spectrum for species Z. The Langevin equation was integrated using the Euler–Maruyama algorithm [10] with time step $\delta_{\tau_1} = 0.0017$ over the time interval $[0, 500]$, starting from the equilibrium point (x^*, y^*, z^*) as the initial condition. The model parameters are the same as those used in figure 1. The vertical dashed lines present in panels (a) and (b) mark the position of the peak predicted by equation (19).

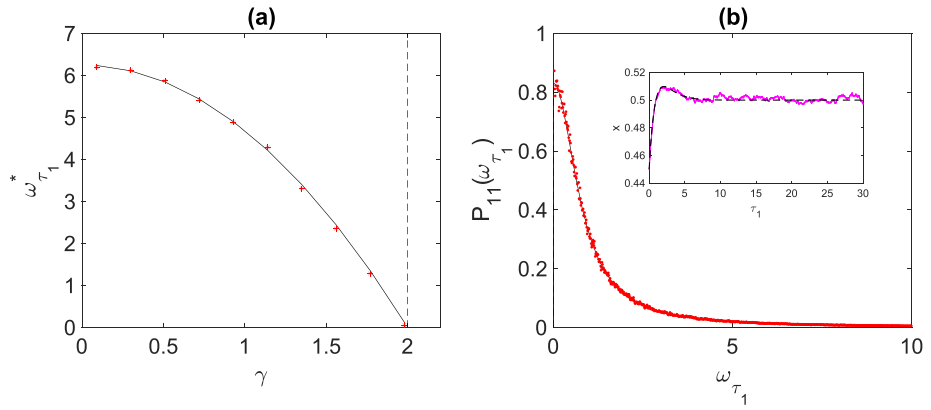


Figure 3. Panel (a): Position of the peak of the power spectrum for species X as a function of γ. The solid line denotes the theoretical prediction given by equation (19) whereas the red dots represent the position of the peak obtained averaging 300 numerical integration of the Langevin equation (12) through the Euler–Maruyama method [10] with time step $\delta\tau_1 = 0.0013$ over the time interval $[0, 500]$. Panel (b): Power spectrum of fluctuation relative to species X for γ close to the critical value δ_z/α_z that is $\gamma = \delta_z/\alpha_z - \varepsilon$ with $\varepsilon = 10^{-6}$. The inset shows a typical stochastic trajectory for species X obtained by numerical integration of the Langevin equation (12) (noisy magenta line) and the deterministic equation (9) (dashed black line) starting from the initial configuration $[0.45, 0.45, 0.4]$. Unspecified parameters are the same as those used in figure 1.

complex eigenvalues associated with the X and Y populations, the eigenvalue corresponding to species Z cannot give rise to noise-induced quasi-cycles.

Let us now focus on the prediction given by equation (19). The position of the peak of the power spectrum, as expected, is modulated both by the ratio between the characteristic sizes of the two families of populations and by the kinetic parameters of species Z. In particular, it is interesting to analyze the dependence of the peak frequency ω_{τ_1} on the parameter γ, which mediates the interaction between species Z and the other two. As can be appreciate by inspection of figure 3(a), the peak position reaches its maximum values as γ approaches 0 (corresponding to the case of two uncoupled families of species), whereas increasing γ up to $\dfrac{\delta_z}{\alpha_z}$, the largest possible value as allowed by condition (10), the peak position tends to zero. From this last observation it is therefore clear that, in the limit

$$\gamma \frac{\alpha_z}{\delta_z} \to 1$$

the effect of species Z on the other two is to inhibit the emergence of quasi-cycles. In this limit, in fact, the power spectra of species X and Y tend to attain their maximum at $\omega_{\tau_1} = 0$, thus losing the periodicity of the generated signal. In figure 3(b) an example of the power spectrum in this limit is shown. In the annexed inset, the corresponding stochastic and deterministic time series for species X is reported:

quasi-cycles are no longer present, as correctly anticipated. Identical considerations naturally apply to species Y.

4. Noise amplification in large neuronal populations

In this section we investigate the limiting case $V >> V_1$, corresponding to a regime in which the neuronal population is much larger than the characteristic size associated with species Z. In this formal limit, we can perform a consistent elimination of the stochastic density referred to species Z to yield a compact system of two coupled stochastic differential equations for the remaining species. We begin by rewriting equation (12) in the original (unscaled) time t yielding:

$$\begin{cases} \dfrac{\mathrm{d}x}{\mathrm{d}t} = \dfrac{1}{V}\left(f(s_x) - x - \gamma xz\right) + \dfrac{1}{\sqrt{V_1}}\dfrac{1}{V}\sqrt{x + \gamma xz + f(s_x)}\ \lambda^{(1)} \\ \dfrac{\mathrm{d}y}{\mathrm{d}t} = \dfrac{1}{V}\left(f(s_y) - y - \gamma yz\right) + \dfrac{1}{\sqrt{V_1}}\dfrac{1}{V}\sqrt{y + \gamma yz + f(s_y)}\ \lambda^{(2)} \\ \dfrac{\mathrm{d}z}{\mathrm{d}t} = \dfrac{1}{V_1}\alpha_z - z\delta_z + \dfrac{1}{\sqrt{V_1}}\dfrac{1}{V_1}\sqrt{z\delta_z + \alpha_z}\ \lambda^{(3)} \end{cases} .$$

Performing the change of variables $\phi_x = \lim_{V\to\infty} x$ and $\phi_y = \lim_{V\to\infty} y$ and introducing the re-scaled time $\tau = t/V$, the previous set of equations becomes

$$\begin{cases} \dfrac{\mathrm{d}\phi_x}{\mathrm{d}\tau} = f(s_{\phi_x}) - \phi_x - \gamma\phi_x z + \dfrac{1}{\sqrt{V_1}}\sqrt{\phi_x + \gamma\phi_x z + f(s_{\phi_x})}\ \lambda^{(1)} \\ \dfrac{\mathrm{d}\phi_y}{\mathrm{d}\tau} = f(s_{\phi_y}) - \phi_y - \gamma\phi_y z) + \dfrac{1}{\sqrt{V_1}}\sqrt{\phi_y + \gamma\phi_y z + f(s_{\phi_y})}\ \lambda^{(2)} \\ \dfrac{\mathrm{d}z}{\mathrm{d}\tau_1} = \alpha_z - z\delta_z + \dfrac{1}{\sqrt{V_1}}\sqrt{z\delta_z + \alpha_z}\ \lambda^{(3)} \end{cases} . \tag{20}$$

Notice that two different time variables appear, τ and $\tau_1 = t/V_1$ defined as in the previous section. This does not pose a problem for the subsequent analysis. We now expand z around its steady state as $z = \bar{z} + \dfrac{1}{\sqrt{V_1}}\xi$ where ξ is a stochastic variable. Substituting this expression into the equation for z in system (20) we obtain

$$\frac{1}{\sqrt{V_1}}\frac{\mathrm{d}\xi}{\mathrm{d}\tau_1} = \alpha_z - \delta_z\left(\bar{z} + \frac{1}{\sqrt{V_1}}\xi\right) + \frac{1}{\sqrt{V_1}}\sqrt{\left(\bar{z} + \frac{1}{\sqrt{V_1}}\xi\right)\delta_z + \alpha_z}\,\lambda^{(3)} . \tag{21}$$

Expanding and neglecting higher-order terms, we match contributions at different orders in $V_1^{-1/2}$. At order $O(1)$ we recover $\bar{z} = \alpha_z/\delta_z \equiv z^*$, while at order $1/\sqrt{V_1}$ we find the stochastic differential equation for ξ

$$\frac{\mathrm{d}\xi}{\mathrm{d}\tau_1} = -\delta_z\xi + \sqrt{2\alpha_z}\,\lambda^{(3)}$$

whose stationary solution is $\xi = \sqrt{\dfrac{\alpha_z}{\delta_z}}\eta$ where η is a random variable from the normal distribution. The above result follows readily from the stationary solution of the Fokker–Planck equation associated to the above linear Langevin equation. Hence:

$$z = \frac{\alpha_z}{\delta_z} + \frac{1}{\sqrt{V_1}}\sqrt{\frac{\alpha_z}{\delta_z}}\,\eta . \tag{22}$$

Substituting equation (22) into the first two equations of system (20), we obtain

$$\begin{cases} \dfrac{\mathrm{d}\phi_x}{\mathrm{d}\tau} = f(s_{\phi_x}) - \phi_x\left(1+\gamma\dfrac{\alpha_z}{\delta_z}\right) + \dfrac{1}{\sqrt{V_1}}\sqrt{\phi_x+\gamma\dfrac{\alpha_z}{\delta_z}\phi_x+\gamma^2\dfrac{\alpha_z}{\delta_z}\phi_x^2+f(s_{\phi_x})}\,\eta \\ \dfrac{\mathrm{d}\phi_x}{\mathrm{d}\tau} = f(s_{\phi_y}) - \phi_y\left(1+\gamma\dfrac{\alpha_z}{\delta_z}\right) + \dfrac{1}{\sqrt{V_1}}\sqrt{\phi_y+\gamma\dfrac{\alpha_z}{\delta_z}\phi_y+\gamma^2\dfrac{\alpha_z}{\delta_z}\phi_y^2+f(s_{\phi_y})}\,\eta \end{cases} . \tag{23}$$

We now assume that ϕ_x and ϕ_y fluctuate around their steady-state values $(x^*, y^*) = (1/2, 1/2)$ and write them as

$$\begin{aligned} \phi_x &= \frac{1}{2} + \frac{1}{\sqrt{V_1}}\xi_x \\ \phi_y &= \frac{1}{2} + \frac{1}{\sqrt{V_1}}\xi_y \end{aligned} \tag{24}$$

and perform an expansion of the non linear terms in equation (23) to leading order in $1/\sqrt{V_1}$ obtaining

$$\begin{aligned} f(s_{\phi_x}) &\approx \frac{1}{1+b} - r\frac{1}{\sqrt{V_1}}\frac{b}{(1+b)^2}\xi_y \\ f(s_{\phi_y}) &\approx \frac{1}{1+b} + r\frac{1}{\sqrt{V_1}}\frac{b}{(1+b)^2}\xi_x \end{aligned} . \tag{25}$$

Substituting equation (25) into equation (23) and retaining only terms up to order $O(1)$ and $O(1/\sqrt{V_1})$ we end up with the following linear Langevin equation

$$\frac{\mathrm{d}}{\mathrm{d}\tau}\begin{pmatrix}\xi_x \\ \xi_y\end{pmatrix} = J\begin{pmatrix}\xi_x \\ \xi_y\end{pmatrix} + \sqrt{1+\gamma\frac{\alpha_z}{\delta_z}+\frac{\gamma^2}{4}\frac{\alpha_z}{\delta_z}}\begin{pmatrix}\eta \\ \eta\end{pmatrix} \tag{26}$$

where J is the 2×2 sub-matrix obtained by removing the third row and the third column from the Jacobian matrix $\mathscr{J}$ defined in equation (11). Comparing (26) with equations (13) and (14) we observe that the noise amplitude is increased by the positive term $\frac{\gamma^2}{4}\frac{\alpha_z}{\delta_z}$ thereby showing that, in the limit of large neuronal populations, the effect of species Z is to enhance the strength of the (finite size) noise.

Also in this case, the power spectrum of the fluctuations can be computed and is found to have the same structure as equation (17):

$$P_{ij}(\omega_{\tau_1}) = \left[1+\gamma\frac{\alpha_z}{\delta_z}+\frac{\gamma^2}{4}\frac{\alpha_z}{\delta_z}\right]\left(\Phi^{-1}\begin{pmatrix}1 & 1\\ 1 & 1\end{pmatrix}\left(\Phi^{-1}\right)^{\dagger}\right)_{ij} \tag{27}$$

where matrix $\Phi = -J - \mathrm{i}\omega_\tau \mathbb{I}_2$ with $\mathbb{I}_2$ is the 2×2 identity matrix. Here indices i and j are limited to $\{1,2\}$. As before, the position of the spectral peak can be estimated by minimizing the denominator, yielding

$$\omega_\tau^* = \left(1+\gamma\frac{\alpha_z}{\delta_z}\right)\sqrt{1+\frac{r^2}{16}\left(1-\gamma\frac{\alpha_z}{\delta_z}\right)^2}. \tag{28}$$

The accuracy of the proposed approximation is confirmed by figure 4 which shows the comparison of the theoretical power spectrum (27) with the analogous quantity obtained by processing the numerical trajectory. This latter is obtained by integrating the Langevin equation (12) for the complete version of the model (i.e. by accounting for the simultaneous presence of the three species) operated in the relevant setting $V >> V_1$. The close agreement between the theoretical prediction and the numerical result shows that the reduced description obtained through the adiabatic elimination of species Z retains the essential features of the stochastic dynamics of the complete three-species model. In particular, the effective two-species description correctly captures the contribution of Z to the fluctuations of the neuronal populations, despite the fact that the dynamics of Z is no longer explicitly represented. This result confirms that the approximation provides a reliable description of the complete model in the limiting regime $V >> V_1$.

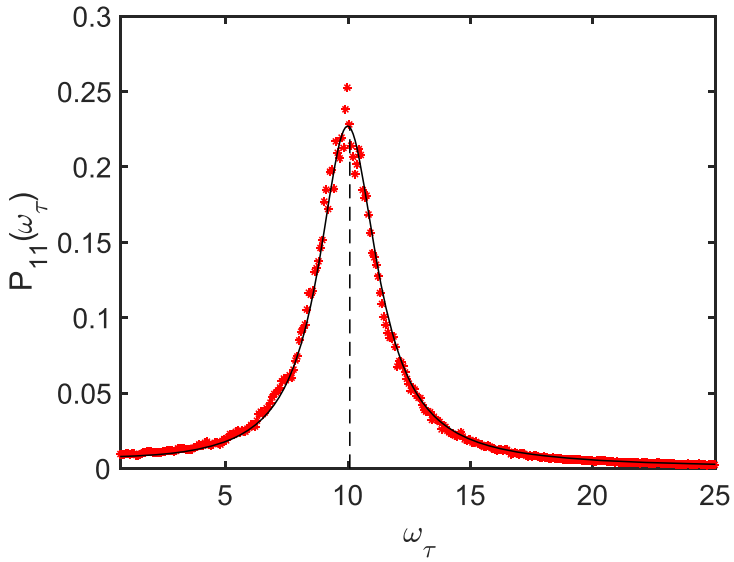


Figure 4. Power spectrum of fluctuations for species X. The solid black line corresponds to the theoretical prediction given by equation (27) while red dots are obtained from numerical integration of the Langevin equation (12) using the Euler–Maruyama algorithm [10] with time step $\delta\tau_1 = 0.0002$ over $2 \cdot 10^7$ steps, and averaged over realizations 200 realizations. The model parameters are $r = 50$, $\gamma = 0.9$, $\delta_z = 0.8$, $\alpha_z = 0.4$, $V_1 = 200$ and $V = 10000$. To enable comparison between the two spectra, frequencies have been rescaled as $\omega_\tau = V/V_1\omega_{\tau_1}$.

5. Conclusion

We have here presented an extension of the model introduced in [28] by including an additional interacting species. We assumed that this new species is characterized by a different intrinsic size scale with respect to the two neuronal populations. This framework allowed us to investigate the role of species Z in two distinct regimes. When the characteristic sizes of the two neuronal populations and species Z are of the same order, the presence of Z modulates the position of the oscillatory peak, up to a limiting case in which oscillations in the neuronal populations disappear altogether. Conversely, when the neuronal populations are assumed to be very large, the effect of the additional species is to enhance the intensity of the stochastic fluctuations, effectively amplifying the strength of the noise. This latter effect is captured analytically by resorting to a simplified two populations setting, which follows a self-consistent stochastic elimination of the third added species. This provides a concrete mechanism by which additional, possibly unresolved, chemical degrees of freedom may influence collective stochastic dynamics.

A natural direction opened by these results is therefore the study of synchronization in networks of noisy oscillators coupled through auxiliary stochastic species. In such systems, the effective noise acting on each oscillator may depend not only on its intrinsic population size but also on the size, dynamics, and coupling of the auxiliary chemical variables. It would consequently be interesting to determine whether the additional source of intrinsic noise identified here can enhance or suppress phase coherence and synchronization, and whether it can lead to synchronization regimes that are absent in the corresponding reduced deterministic or purely neuronal descriptions. This would extend the classical Kuramoto picture by incorporating dynamically generated and chemically mediated fluctuations as an additional control mechanism for collective synchronization.

Acknowledgments

Francesca Di Patti thanks Gruppo Nazionale di Fisica Matematica (GNFM) of Istituto Nazionale di Alta Matematica (INDAM) for partial financial support.

Data availability statements

The data that support the findings of this study are openly available at the following URL/DOI: https://doi.org/10.5281/zenodo.20704833 [29].

Funding

The work by Duccio Fanelli is supported by NEXTGENERATIONEU (NGEU) and funded by the Ministry of University and Research (MUR), National Recovery and Resilience Plan (NRRP), project MNESYS (PE0000006) 'A Multiscale integrated approach to the study of the nervous system in health and disease' (DR. 1553 11.10.2022).

Author contributions

Francesca Di Patti 0000-0003-1288-0079
Conceptualization (equal), Formal analysis (equal), Investigation (equal), Methodology (equal), Project administration (equal), Software (equal), Supervision (equal), Validation (equal), Visualization (equal), Writing – original draft (equal), Writing – review & editing (equal)

Duccio Fanelli 0000-0001-8545-9424
Conceptualization (equal), Formal analysis (equal), Investigation (equal), Methodology (equal), Project administration (equal), Software (equal), Supervision (equal), Validation (equal), Visualization (equal), Writing – original draft (equal), Writing – review & editing (equal)

Perla Rosi 0009-0000-4631-5735
Conceptualization (supporting), Formal analysis (equal), Investigation (equal), Software (equal), Validation (equal), Writing – original draft (supporting)

Appendix A. System-size expansion of the master equation

The explicit form of equation (5) reads

$$\begin{aligned}\frac{\mathrm{d}P}{\mathrm{d}t}(\mathbf{n},t) = {} & T\left(\mathbf{n}|n_x+1,n_y,n_z\right)P\left(n_x+1,n_y,n_z,t\right)\\ & + T\left(\mathbf{n}|n_x,n_y+1,n_z\right)P\left(n_x,n_y+1,n_z,t\right)\\ & + T\left(\mathbf{n}|n_x,n_y,n_z+1\right)P\left(n_x,n_y,n_z+1,t\right)\\ & + T\left(\mathbf{n}|n_x-1,n_y,n_z\right)P\left(n_x-1,n_y,n_z,t\right)\\ & + T\left(\mathbf{n}|n_x,n_y-1,n_z\right)P\left(n_x,n_y-1,n_z,t\right)\\ & + T\left(\mathbf{n}|n_x,n_1,n_z-1\right)P\left(n_x,n_y,n_z-1,t\right)\\ & - T\left(n_x+1,n_y,n_z|\mathbf{n}\right)P(\mathbf{n},t) - T\left(n_x,n_y+1,n_z|\mathbf{n}\right)P(\mathbf{n},t)\\ & - T\left(n_x,n_y,n_z+1|\mathbf{n}\right)P(\mathbf{n},t) - T\left(n_x-1,n_y,n_z|\mathbf{n}\right)P(\mathbf{n},t)\\ & - T\left(n_x,n_y-1,n_z|\mathbf{n}\right)P(\mathbf{n},t) - T\left(n_x,n_y,n_z-1|\mathbf{n}\right)P(\mathbf{n},t).\end{aligned} \tag{29}$$

Introducing the step operators

$$\begin{aligned}\epsilon_x^{\pm}g\left(n_x,n_y,n_z\right) &= g\left(n_x\pm1,n_y,n_z\right),\\ \epsilon_y^{\pm}g\left(n_x,n_y,n_z\right) &= g\left(n_x,n_y\pm1,n_z\right),\\ \epsilon_z^{\pm}g\left(n_x,n_y,n_z\right) &= g\left(n_x,n_y,n_z\pm1\right)\end{aligned}$$

where $g(n_x,n_y,n_z)$ is a generic function, the master equation can be written in compact form as

$$\begin{aligned}\frac{\mathrm{d}P}{\mathrm{d}t}(\mathbf{n},t) = {} & \left[\left(\epsilon_x^{+}-1\right)T\left(n_x-1,n_y,n_z|\mathbf{n}\right)+\left(\epsilon_x^{-}-1\right)T\left(n_x+1,n_y,n_z|\mathbf{n}\right)\right]P(\mathbf{n},t)\\ & + \left[\left(\epsilon_y^{+}-1\right)T\left(n_x,n_y-1,n_z|\mathbf{n}\right)+\left(\epsilon_y^{-}-1\right)T\left(n_x,n_y+1,n_z|\mathbf{n}\right)\right]P(\mathbf{n},t)\\ & + \left[\left(\epsilon_z^{+}-1\right)T\left(n_x,n_y,n_z-1|\mathbf{n}\right)+\left(\epsilon_z^{-}-1\right)T\left(n_x,n_y,n_z+1|\mathbf{n}\right)\right]P(\mathbf{n},t).\end{aligned} \tag{30}$$

We now perform the system-size expansion. To this end we introduce the new variables $x=\frac{n_x}{V}$, $y=\frac{n_y}{V}$ and $z=\frac{n_z}{V_1}$ so that the step operators can be expressed as

$$\epsilon_x^{\pm} g(x,y,z) = g\left(x \pm \frac{1}{V}, y, z\right)$$
$$\epsilon_y^{\pm} g(x,y,z) = g\left(x, y \pm \frac{1}{V}, z\right)$$
$$\epsilon_z^{\pm} g(x,y,z) = g\left(x, y, z \pm \frac{1}{V_1}\right)$$

and, in the limit of large volumes, we can expand the step operators in powers of $1/\sqrt{V}$ and $1/\sqrt{V_1}$ as

$$\begin{aligned}
\epsilon_x^{\pm} &\approx 1 \pm \frac{1}{V}\frac{\partial}{\partial x} + \frac{1}{2V^2}\frac{\partial^2}{\partial x^2} \\
\epsilon_y^{\pm} &\approx 1 \pm \frac{1}{V}\frac{\partial}{\partial y} + \frac{1}{2V^2}\frac{\partial^2}{\partial y^2} \\
\epsilon_z^{\pm} &\approx 1 \pm \frac{1}{V_1}\frac{\partial}{\partial z} + \frac{1}{2V_1^2}\frac{\partial^2}{\partial z^2}.
\end{aligned} \tag{31}$$

Inserting (31) into (30) we get

$$\begin{aligned}
\frac{\mathrm{d}P}{\mathrm{d}t}(x,y,z,t) = &\frac{1}{V}\frac{\partial}{\partial x}\left[(T(n_x-1,n_y,n_z|\mathbf{n}) - T(n_x+1,n_y,n_z|\mathbf{n}))P(\mathbf{n},t)\right] \\
&+ \frac{1}{V}\frac{\partial}{\partial y}\left[(T(n_x,n_y-1,n_z|\mathbf{n}) - T(n_x,n_y+1,n_z|\mathbf{n}))P(\mathbf{n},y)\right] \\
&+ \frac{1}{V_1}\frac{\partial}{\partial z}\left[(T(n_x,n_y,n_z-1|\mathbf{n}) - T(n_x,n_y,n_z+1|\mathbf{n}))P(\mathbf{n},t)\right] \\
&+ \frac{1}{2V^2}\frac{\partial^2}{\partial x^2}\left[(T(n_x-1,n_y,n_z|\mathbf{n}) + T(n_x+1,n_y,n_z|\mathbf{n}))P(\mathbf{n},t)\right] \\
&+ \frac{1}{2V^2}\frac{\partial^2}{\partial y^2}\left[(T(n_x,n_y-1,n_z|\mathbf{n}) + T(n_x,n_y+1,n_z|\mathbf{n}))P(\mathbf{n},t)\right] \\
&+ \frac{1}{2V_1^2}\frac{\partial^2}{\partial z^2}\left[T(n_x,n_y,n_z-1|\mathbf{n}) + T(n_x,n_y,n_z+1|\mathbf{n}))P(\mathbf{n},t)\right].
\end{aligned}$$

that, introducing the vector $\mathbf{k} = (x,y,z)$ and rescaling time as $\tau_1 = \dfrac{t}{V_1}$, can be rewritten as the following Fokker–Planck equation

$$\frac{\mathrm{d}P}{\mathrm{d}\tau_1}(\mathbf{k},t) = -\sum_{i=1}^{3}\frac{\partial}{\partial k_i}A_i P(\mathbf{n},t) + \sum_{i=1}^{3}\frac{1}{2V_1}\frac{\partial^2}{\partial k_i^2}B_i P(\mathbf{n},t) \tag{32}$$

with

$$\mathbf{A} = \begin{pmatrix} \dfrac{V_1}{V}\left(T\left(n_x+1,n_y,n_z|\mathbf{n}\right) - T\left(n_x-1,n_y,n_z|\mathbf{n}\right)\right) \\ \dfrac{V_1}{V}\left(T\left(n_x,n_y+1,n_z|\mathbf{n}\right) - T\left(n_x,n_y-1,n_z|\mathbf{n}\right)\right) \\ T\left(n_x,n_y,n_z+1|\mathbf{n}\right) - T\left(n_x,n_y,n_z-1,|\mathbf{n}\right) \end{pmatrix}$$

and

$$\mathbf{B} = \begin{pmatrix} \dfrac{V_1^2}{V^2}\left(T\left(n_x-1,n_y,n_z|\mathbf{n}\right) + T\left(n_x+1,n_y,n_z|\mathbf{n}\right)\right) \\ \dfrac{V_1^2}{V^2}\left(T\left(n_x,n_y-1,n_z|\mathbf{n}\right) + T\left(n_x,n_y+1,n_z|\mathbf{n}\right)\right) \\ T\left(n_x,n_y,n_z-1|\mathbf{n}\right) + T\left(n_x,n_y,n_z+1|\mathbf{n}\right) \end{pmatrix}. \tag{33}$$

Equation (32) admits the following equivalent Langevin representation

$$\begin{cases} \dfrac{\mathrm{d}x}{\mathrm{d}\tau_1} = \dfrac{V_1}{V}\left(T\left(n_x+1,n_y,n_z|\mathbf{n}\right) - T\left(n_x-1,n_y,n_z|\mathbf{n}\right)\right) + \dfrac{1}{\sqrt{V_1}}\rho^{(1)} \\ \dfrac{\mathrm{d}y}{\mathrm{d}\tau_1} = \dfrac{V_1}{V}\left(T\left(n_x,n_y+1,n_z|\mathbf{n}\right) - T\left(n_x,n_y-1,n_z|,\mathbf{n}\right)\right) + \dfrac{1}{\sqrt{V_1}}\rho^{(2)} \\ \dfrac{\mathrm{d}z}{\mathrm{d}\tau_1} = T\left(n_x,n_y,n_z+1|\mathbf{n}\right) - T\left(n_x,n_y,n_z-1|\mathbf{n}\right) + \dfrac{1}{\sqrt{V_1}}\rho^{(3)} \end{cases} \tag{34}$$

where $\boldsymbol{\rho} = (\rho^{(1)}, \rho^{(2)}, \rho^{(3)})$ is a stochastic vector whose components have zero mean and correlator $\langle \rho^{(\ell)}(\tau_1)\rho^{m}(\tau_1')\rangle = B_\ell \delta_{\ell m}\delta(\tau_1 - \tau_1')$. It is convenient to express the noise in terms of Gaussian white noise with unit variance. To this end, we introduce $\boldsymbol{\lambda} = (\lambda^{(1)}, \lambda^{(2)}, \lambda^{(3)})$, satisfying

$$\begin{aligned} \langle \lambda^{(\ell)} \rangle &= 0 \\ \langle \lambda^{(\ell)}(\tau_1)\, \lambda^{(m)}(\tau_1')\rangle &= \delta_{\ell m}\delta(\tau_1 - \tau_1') \end{aligned} \quad .$$

Denoting by $\mathscr{B}$ the diagonal diffusion matrix, with entries $\mathscr{B}_{ij} = B_i\delta_{ij}$ with $\mathbf{B}$ given by equation (33), we perform the change of variables $\boldsymbol{\rho} = G\boldsymbol{\lambda}$ where the matrix G is defined such that $\mathscr{B} = GG^t$. In this case G is diagonal with entries

$$\mathrm{diag}G = \begin{pmatrix} \dfrac{V_1}{V}\sqrt{T\left(n_x-1,n_y,n_z|\mathbf{n}\right) + T\left(n_x+1,n_y,n_z|\mathbf{n}\right)} \\ \dfrac{V_1}{V}\sqrt{T\left(n_x,n_y-1,n_z|\mathbf{n}\right) + T\left(n_x,n_y+1,n_z|\mathbf{n}\right)} \\ \sqrt{T\left(n_x,n_y,n_z-1|\mathbf{n}\right) + T\left(n_x,n_y,n_z+1|\mathbf{n}\right)} \end{pmatrix} \quad .$$

With this transformation, the Langevin equation (34) can be recast in the form of equation (12).

Appendix B. Linear noise approximation

We now expand the nonlinear terms in equation (12) in powers of $V_1^{-1/2}$. The arguments of the sigmoid functions become

$$\begin{aligned} s_x &= -r\frac{\xi_y}{\sqrt{V_1}} \\ s_y &= r\frac{\xi_x}{\sqrt{V_1}} \end{aligned}$$

which yield, at first order,

$$\begin{aligned} f(s_x) &\approx f(0) + f'(0)\left(-r\frac{\xi_y}{\sqrt{V_1}}\right) = \frac{1}{1+b} - r\frac{b}{(1+b)^2}\frac{\xi_y}{\sqrt{V_1}} \\ f(s_y) &\approx f(0) + f'(0)\left(r\frac{\xi_x}{\sqrt{V_1}}\right) = \frac{1}{1+b} + r\frac{b}{(1+b)^2}\frac{\xi_x}{\sqrt{V_1}} \end{aligned} \quad .$$

Neglecting higher-order terms in $V_1^{-1/2}$, equation (12) reduces to

$$\begin{aligned} &\sqrt{x + \gamma xz + f(s_x)} \approx \sqrt{\frac{1}{2} + \frac{\gamma\alpha_z}{2\delta_z} + \frac{1}{1+b}} = \sqrt{1+\gamma\frac{\alpha_z}{\delta_z}}, \\ &\sqrt{y + \gamma yz + f(s_y)} \approx \sqrt{\frac{1}{2} + \frac{\gamma\alpha_z}{2\delta_z} + \frac{1}{1+b}} = \sqrt{1+\gamma\frac{\alpha_z}{\delta_z}}, \sqrt{z\delta_z + \alpha_z} \approx \sqrt{2\alpha_z}. \end{aligned}$$

In this way, neglecting higher order terms with respect to $\frac{1}{\sqrt{V_1}}$, equation (12) becomes

$$\begin{cases} \dfrac{\mathrm{d}\xi_x}{\mathrm{d}\tau_1} = \dfrac{V_1}{V}\left[\xi_x\left(-1-\gamma\dfrac{\alpha_z}{\delta_z}\right) - \xi_y\dfrac{r}{4}\left(1-\gamma^2\dfrac{\alpha_z^2}{\delta_z^2}\right) - \dfrac{\gamma}{2}\xi_z\right] + \dfrac{V_1}{V}\sqrt{1+\gamma\dfrac{\alpha_z}{\delta_z}}\ \lambda^{(1)} \\ \dfrac{\mathrm{d}\xi_y}{\mathrm{d}\tau_1} = \dfrac{V_1}{V}\left[\xi_x\dfrac{r}{4}\left(1-\gamma^2\dfrac{\alpha_z^2}{\delta_z^2}\right) + \xi_y\left(-1-\gamma\dfrac{\alpha_z}{\delta_z}\right) - \dfrac{\gamma}{2}\xi_z\right] + \dfrac{V_1}{V}\sqrt{1+\gamma\dfrac{\alpha_z}{\delta_z}}\ \lambda^{(2)} \\ \dfrac{\mathrm{d}\xi_z}{\mathrm{d}\tau_1} = -\delta_z\xi_z + \sqrt{2\alpha_z}\ \lambda^{(3)} \end{cases} \tag{35}$$

that corresponds to the extended version of equation (13).

References

[1] Acebron J A, Bonilla L L, Pérez Vicente C J, Ritort F and Spigler R 2005 The kuramoto model: a simple paradigm for synchronization phenomena *Rev. Mod. Phys.* **77** 137
[2] Biancalani T, Fanelli D and Di Patti F 2010 Stochastic turing patterns in the brusselator model *Phys. Rev. E* **81** 046215
[3] Boison D 2008 Adenosine as a neuromodulator in neurological diseases *Curr. Opin. Pharmacol.* **8** 2–7
[4] Bressloff P C and Maclaurin J N 2018 Stochastic hybrid systems in cellular neuroscience *J. Math. Neurosci.* **8** 1–71
[5] Cowan J D, Neuman J and van Drongelen W 2016 Wilson–Cowan equations for neocortical dynamics *J. Math. Neurosc.* **6** 643–53
[6] Di Patti F, Lavacchi L, Arbel-Goren R, Schein-Lubomirsky L, Fanelli D and Stavans J 2018 Robust stochastic turing patterns in the development of a one-dimensional cyanobacterial organism *PLOS Biol.* **16** e2004877
[7] Dunwiddie T V and Masino S A 2001 The role and regulation of adenosine in the central nervous system *Annu. Rev. Neurosci.* **24** 31–55
[8] Fanelli D, Ginelli F, Livi R, Zagli N and Zankoc C 2017 Noise-driven neuromorphic tuned amplifier *Phys. Rev. E* **96** 062313
[9] Kandel E R, Schwartz J H and Jessell T M 2000 *Principles of Neural Science* 4th edn (McGraw-Hill)
[10] Kloeden P E and Platen E 1992 *Numerical Solution of Stochastic Differential Equations* (Springer)
[11] Kuramoto Y 1984 *Chemical Oscillations, Waves and Turbulence* (Springer)
[12] Lecca P, Bagagiolo F and Scarpa M 2017 Hybrid deterministic/stochastic simulation of complex biochemical systems *Mol. BioSyst.* **13** 2672–86
[13] Linden J M 1999 *Basic Neurochemistry: Molecular, Cellular and Medical Aspects.*, *Chapter Purine Release and Metabolism* 6th edn (Lippincott-Raven)
[14] McKane A J and Newman T J 2005 Predator-prey cycles from resonant amplification of demographic stochasticity *Phys. Rev. Lett.* **94** 218102
[15] Pahle J 2009 Biochemical simulations: stochastic, approximate stochastic and hybrid approaches *Brief. Bioinform.* **10** 53–64
[16] Parra-Rojas C, Fanelli D and McKane A J 2026 Stochastic quasi-cycles as a simple explanation for the time evolution of the cape rodney-okakari point marine ecological reserve *Ecol. Model.* **514** 111477
[17] Di Patti F, Arbel-Goren R, Fanelli D and Stavans J 2026 Demographic noise induced patterns in space and time *Phys. Rep.* **1179** 1–64
[18] Di Patti F, Chirino Y U, Arbel-Gorent R, Sharon T, Castillo A, Alvarez-Buylla E, Fanelli D and Stavans J 2023 Stochastic turing patterns of trichomes in arabidopsis leaves *Proc. Natl Acad. Sci.* **120** e2309616120
[19] Pikovsky A, Rosenblum M and Kurths J 2001 *Synchronization: A universal Concept in Nonlinear Sciences (Cambridge Nonlinear Science Series)* (Cambridge University Press)
[20] Purves D, Augustine G J, Fitzpatrick D, Katz L C, LaMantia A, McNamara J O and Williams S M 2001 *Neuroscience* 2nd edn (Synaptic Transmission. Sinauer Associates Inc.)
[21] Strogatz S H 2000 From kuramoto to crawford: exploring the onset of synchronization in populations of coupled oscillators *Physica D* **143** 1–20
[22] Strogatz S H 2003 *Sync: The Emerging Science of Spontaneous Order* (Hyperion)
[23] Wilson H R and Cowan J D 1972 Excitatory and inhibitory interactions in localized populations of model neurons *Biophys. J.* **12** 1–24
[24] Wilson H R and Cowan J D 1973 A mathematical theory of the functional dynamics of cortical and thalamic nervous tissue *Cybernetik* **13** 55–80
[25] Wilson H R and Cowan J D 2021 Evolution of the Wilson–Cowan equations *Biol. Cybern* **115** 643–53
[26] Wylie D C, Hori Y, Dinner A R and Chakraborty A K 2006 A hybrid deterministic-stochastic algorithm for modeling cell signaling dynamics in spatially inhomogeneous environments and under the influence of external fields *J. Phys. Chem B* **110** 12749–65
[27] Kuramoto Y Y 1975 Self-entrainment of a population of coupled non-linear oscillators *International Symposium on Mathematical Problems in Theoretical Physics* vol 39, ed H Araki (Springer) pp 420–2
[28] Zankoc C, Fanelli D, Ginelli F and Livi R 2017 Intertangled stochastic motifs in networks of excitatory-inhibitory units *Phys. Rev. E* **96** 022308
[29] Di Patti F, Fanelli D and Rosi P 2026 Custom code for the paper "Noise seeded oscillators: on the role of demographic fluctuations in a multi-populations model" *Zenodo* https://doi.org/10.5281/zenodo.20704833